Communication

Phenomenological plasmon broadening and relation to the dispersion

CrossMark

Raphael Hobbiger*, Jürgen T. Drachta, Dominik Kreil, Helga M. Böhm

Institute for Theoretical Physics Johannes Kepler University A-4040 Linz, Austria

ARTICLE INFO

ABSTRACT

Pragmatic ways of including lifetime broadening of collective modes in the electron liquid are critically compared. Special focus lies on the impact of the damping parameter onto the dispersion. It is quantitatively exemplified for the two-dimensional case, for both, the charge ('sheet'-)plasmon and the spin-density plasmon. The predicted deviations fall within the resolution limits of advanced techniques.

1. Introduction

The study of plasmons, the collective oscillations of electrons, has a long and successful history [1,2]. Their coupling to light in nano-structures, known as 'plasmonics', holds high promise for revolutionary applications [3], where the performance of actual devices is crucially limited by metallic losses [4]. An undemanding inclusion of a plasmon's damping via a constant, irrespective of the losses' origin(s), is commonly achieved via a Drude type dielectric function [2]. The response of charges, however, is nonlocal, which is the more important the smaller the size of the nanoparticles is.

The random phase approximation (RPA) [2], historically a milestone, provides a dielectric function explicitly depending on both, frequency ω as well as wave vector q. Its failure to include finite lifetime effects was treated early by Mermin [5], his approach still being widely applied. Recent examples in bulk systems include calculations of the electrons' inelastic mean free path [6], stopping power [7], and a generalization to spin wave damping [8]. In layers, it has been employed, e.g., to obtain quasi-particle properties [9] of the two-dimensional electron gas (2Deg), or when accounting for inter-band-excitation losses in graphene [10].

Major techniques for studying the charge response to external perturbations are scattering experiments [11] and, for long wave-lengths, optical measurements. They yield the same dispersion *only* for an undamped plasmon; for realistic lifetimes slightly different results are obtained.[1] This discrepancy in the plasmon *dispersion* $\omega_{pl}(q)$ increases with its linewidth (often broadening with q). Consequently, comparing theory and high-resolution experiments needs appropriate caution.

Forefront scattering data for dispersion and damping are known for metallic monolayers [12–14] and semiconductor quantum wells

[15,16]. Many 2Degs being rather dense [17], RPA predictions are sufficiently accurate, once damping effects are built in effectively. The 2Deg, our prototype, shares the vanishing of $\omega_{pl}(q \to 0)$ with graphene. There, too, the plasmon was studied with optical as well as scattering methods [18–22] (plasmons in graphene are thoroughly reviewed in [23,24]).

Mermin's approach conserves the local electron number, invoking just a single additional constant η (the inverse lifetime τ). Extensions further conserving local energy and momentum were developed (and applied to a two-component plasma) by Röpke [25–27], and, independently, by Atwal and Ashcroft [28]. These sophisticated theories yield intricate response functions with a wave vector dependent linewidth, as also found in [29]. But in view of realistic materials an uncomplicated RPA extension incorporating plasmon lifetimes via a phenomenological (potentially q-dependent) parameter is preferential. Describing damping irrespective of the microscopic mechanism(s), phenomenological life times can be taken from both, experiments or published data from theories, which cannot be easily recreated.

The purpose of this work is to critically compare other simple approaches with that of Mermin, and to study the resulting plasmon dispersions. Deviations from the classical plasma frequency, ω_p, turn out larger than expected.

After briefly discussing general aspects in Section 2, we present quantitative (zero temperature) results (both in RPA and beyond) in Section 3 for a 2Deg. There, the vanishing of $\omega_{pl}(q \to 0)$ implies a comparably high relative width, also in case of rather weak damping. Finally, we study the spin-density plasmon in the partially spin-polarized case in Section 4. For Fourier Transforms conventions are as in [1].

---

* Corresponding author.
  E-mail address: raphael.hobbiger@jku.at (R. Hobbiger).
  [1] For the Drude case this was already noted in [2, p.207f.],

2. Theoretical overview

A plasmon is conventionally obtained from the complex dielectric function $\epsilon = \epsilon_I + i\,\epsilon_{II}$ via these, closely related but not exactly equal definitions:

- as a maximum in the double differential scattering cross section [12,16],

$$\text{Im}\frac{-1}{\epsilon(q,\omega_{pl}^{(a)})} = \text{max};\tag{1a}$$

- as the vanishing of the complex ϵ for complex ω [28], determining reflection coefficients (purely oscillatory waves change to decaying ones)

$$\epsilon(q,\omega_I + i\omega_{II}) = 0,\quad \omega_{pl}^{(b)} \equiv \omega_I;\tag{1b}$$

- often approximated as the zero of Re ϵ with real frequencies [21],

$$\epsilon_I(q,\omega_{pl}^{(c)}) = 0;\tag{1c}$$

(the approximation being justified if $\omega_I \gg \omega_{II}$, and $\omega_{pl}^{(c)}$ is always lower than $\omega_{pl}^{(a,b)}$ [30]),

- or, if the phase shift is not relevant, as minimal magnitude of ϵ (implying a maximal electric field),

$$|\epsilon(q,\omega_{pl}^{(d)})| = \text{min}.\tag{1d}$$

The Drude model [2] for charge carriers with a classical plasma frequency ω_p reads $\epsilon_{Dru}(q,\omega) = 1 - \omega_p^2/\omega(\omega + i\eta)$. Here, $\omega_{pl}^{(a)}$ and $\omega_{pl}^{(b)}$ differ <1% for η even as large as ω_p, but conditions (1c–1d) yield clearly distinct values, unless η is rather small. The criterion appropriate to the setup must be chosen for cutting edge experimental resolutions. Typical values reported [12,14] are $\sim$10 meV (roughly 10% of ω_{pl}), $\sim$25…125 meV $\approx$ 10…50% of ω_{pl} [19] and $\sim$ 100 meV [31]. By definition, (1a) yields a symmetric Lorentzian near $\omega_{pl}^{(a)}$, whereas expansions around $\omega_{pl}^{(b-d)}$ contain first order terms in the denominator, too:

$$\text{Im}\frac{-1}{\epsilon(q,\omega)} \approx \begin{cases} \dfrac{\alpha}{\left(\omega - \omega_{pl}^{(a)}\right)^2 + \gamma^2} \\[2ex] \dfrac{\alpha}{\left(\omega - \omega_{pl}^{(b-d)}\right)^2 + \beta\left(\omega - \omega_{pl}^{(b-d)}\right) + \gamma^2} \end{cases}.\tag{2}$$

Clearly, the discrepancy in differently computed ω_{pl}-values depends on the specific $\epsilon(q,\omega)$ used. Some common forms are given next.

The linear response of an electron liquid to external perturbations in RPA-type approaches reads

$$\epsilon_{RPA}(q,\omega) = 1 - v(q)\chi^0(q,\omega);\tag{3}$$

here, $v(q)$ denotes the Coulomb interaction, and $\chi^0(q,\omega)$ the density–density response function of non-interacting fermions [1]. It shows the typical electron–hole (e/h) excitation band in the (q,ω)-plane. An adiabatically turned on perturbation corresponds to $\omega \to \omega + i0^+$. This ensures causality, but yields an undamped plasmon. An obvious idea to include damping is to use $\chi^0(q,\tilde\omega)$ with $\tilde\omega \equiv \omega + i\eta$ and inverse lifetime $\eta \equiv 1/\tau$,

$$\epsilon_{Lin}(q,\omega) \equiv 1 - v(q)\chi^0(q,\tilde\omega).\tag{4}$$

This also broadens the e/h band (as $\text{Im}\chi^0(q,\tilde\omega)$, at any q, only vanishes when $|\omega\tau| \gg 1$). It catches the eye that Eq. (4) alters the static response

$$\epsilon_{Lin}(q,0) = 1 - v(q)\chi^0(q,i\eta) \xrightarrow{q\to 0} 1 + \omega_p^2/\eta^2\tag{5}$$

violating $\epsilon(q\to 0,\ 0) = 1 + v(q)N(E_F)$ (the perfect screening sum rule, $N(E_F)$ is the density of states at the Fermi energy). The correctness of

this limit may be of less importance for plasmonic applications, which are far from static.

Mermin [5] corrected the deficiency. He deriv"ed

$$\epsilon_{Me}(q,\omega) \equiv 1 - \frac{v(q)\chi^0(q,\tilde\omega)}{1 + i\eta g_{Me}(q,\tilde\omega)};\tag{6a}$$

$$g_{Me}(q,\tilde\omega) \equiv \frac{1}{\tilde\omega}\left(\frac{\chi^0(q,\tilde\omega)}{\chi^0(q,0)} - 1\right).\tag{6b}$$

Albeit elegant, analytical calculations with Eq. (6) quickly get cumbersome, in particular when the relations are meant as matrix equations (2×2 for spin-dependent screening or electron–hole liquids, infinite matrices in reciprocal lattice vectors of crystals). Note that (6b) does *not* yield, as it should, the classical plasmon for long wavelengths,

$$\omega_{pl}^{(b)}(q\to 0)_{Me} \nrightarrow \omega_p,\tag{7}$$

neither in the bulk nor for the 2Deg [28] (there, also $\omega_{pl}^{(a)}(q\to 0)$ shows a mismatch with the $\sqrt{q}$– dependence, cf. Fig. 1).

Comparing approaches with the structure of (6a) but arbitrary ω instead of $\tilde\omega$ is worthwhile,

$$\epsilon_g(q,\omega) \equiv 1 - \frac{v(q)\chi^0(q,\omega)}{1 + i\eta g(q,\omega)}.\tag{8}$$

The elementary choice $g_I \equiv \text{sgn}(\omega_I)\hbar/E_F$ (i.e. simply adding a constant to the RPA's susceptibility denominator, with a sign function for proper symmetry), serves to enhance a long-lived plasmon's visibility in graphical representations. The dielectric function with $g_D \equiv 1/\omega$ reduces to the Drude model for $\omega \gg \hbar q^2/2m$ (m is the effective electron mass). For the optical conductivity σ this implies

$$\sigma(\omega) = \frac{ne^2\tau/m}{\omega(g(0,\omega)-i\tau)} \xrightarrow{g=g_D} \frac{ne^2\tau/m}{1-i\omega\tau}.\tag{9}$$

To achieve an interpolation between static RPA screening and the Drude case we propose the form

$$g_{E_F}(\omega) \equiv \frac{\omega}{\omega^2 + E_F^2/\hbar^2}.\tag{10}$$

The main deficiency of this ansatz is to violate the *f*-sum rule (due to additional poles at $\hbar\omega = \pm iE_F$),

$$\int_0^\infty \frac{d\omega}{\pi}\,\omega\,\text{Im}\frac{-1}{\epsilon(q,\omega)} = \frac{\omega_p^2}{2}.\tag{11}$$

When the focus lies on plasmon properties (e.g. the q-dependence), this can be acceptable: No large frequency range (often inaccessible anyhow [32]) needs to be measured for comparing peak positions and widths.

Both, ϵ_{Me} and ϵ_{Lin} fulfill Eq. (11), for the latter occasionally reported otherwise [7]. The contour for the integration (11) in the complex (ω_I,ω_{II})-plane is taken along the quarter circle enclosing the first quadrant. For a purely real integration kernel on the ω_{II}-axis only the arc contributes, provided Im ϵ^{-1} is analytic in the upper half plane (as it should) [1]. The RPA response function obeys these conditions. From its high frequency expansion,

$$\epsilon_{RPA}(q\to 0, |\omega|\to\infty) \approx 1 - \omega_p^2/|\omega|^2,\tag{12}$$

it follows that ϵ_{Lin} also fulfills the *f*-sum rule. While state-of-the-art approaches [25–28] satisfy the widest set of sum rules and treat electron correlations properly, impurity scattering still has to be accounted for phenomenologically.

Note that the static structure factors $S(q)$ obtained from the above dielectric functions via

$$\int_0^\infty \frac{d(\hbar\omega)}{\pi}\text{Im}\frac{-1}{\epsilon(q,\omega)} = v(q)S(q)\tag{13}$$

differ for each approach. For a meaningful comparison of scattering intensities, their normalization by $S(q\to 0)$ appears advisable.

Table 1

Exact criteria, satisfied (✓) or not (×) by the discussed approaches in an electron gas. In Cols.1-5 (positive absorbance, real-valuedness on the imaginary ω-axis, causality, static response, f-sum rule) q is arbitrary. Whether the $q \to 0$ plasmon coincides with the classical ω_p, Col. 6, differs in 2D and 3D for the criteria Eq. (1a) and (1b).

crit./ appr.	$\mathrm{Im}\,\epsilon$ >0	$\epsilon(q, i\omega_{\mathrm{II}})$ $\in \mathbb{R}$	caus.	$\omega = 0$	f–SR	$\omega_p^{\mathrm{class}}$ $\omega_{\mathrm{pl}}^{(a)}$	$\omega_{\mathrm{pl}}^{(b)}$
ϵ_{Dru}	✓	✓	✓	×	✓		
$\epsilon_{\mathrm{Lin}}^{2,3D}$	✓	✓	✓	×	✓	×	✓
$\epsilon_{\mathrm{Me}}^{2,3D}$	✓	✓	✓	✓	✓	×	×
$\epsilon_{g_1}^{2,3D}$	×	×	✓	×	×	×	×
$\epsilon_{g_D}^{2,3D}$	×	✓	✓	×	✓	×	×
$\epsilon_{g_{E_F}}^{2D}$	×	✓	×	✓	×	✓	✓
$\epsilon_{g_{E_F}}^{3D}$	×	✓	×	✓	×	×	×

We point out that η, entering as a parameter, does not necessarily coincide with the half width of the plasmon peak. Only for ϵ_{Lin} the difference is small. In particular, when the half width gets comparable with the distance between $\hbar\omega_{\mathrm{pl}}(q)$ and the e/h-band, the agreement is worse.

Table 1 summarizes the behavior of (4), (6), and (8) with the choices listed above for g. Neither is fully satisfactory. As well-known [1], static and dynamic properties are not easily compatible. Trying to extend the validity of Drude's model by replacing ω_p^2/ω^2 with $v\chi^0/(1 - ig_D)$ fails due to the $1/\omega$ divergence in $g_D(\omega \to 0)$. Although
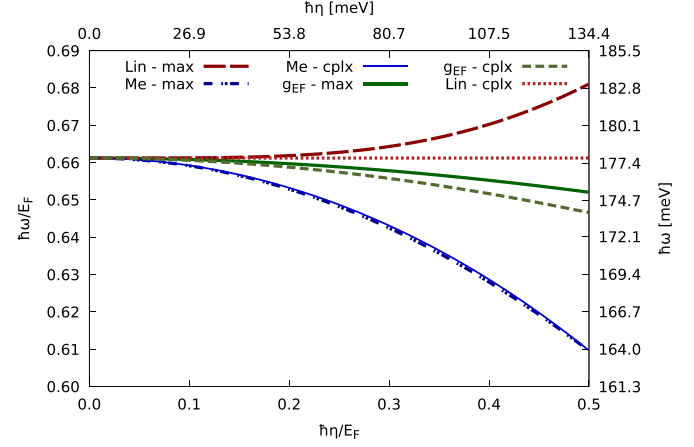

Fig. 2. (Color online) Plasmon dispersion $\omega_{\mathrm{pl}}(q = 0.1\,k_F)$ vs. inverse half width, at $r_S = 1.44$. Note the restricted ω scale. Line styles are the same as in Fig. 1.

g_{E_F} vanishes linearly for low ω, (10) has severe shortcomings where $\mathrm{Re}\,\chi^0(q, \omega)$ changes sign.

In case of a soft $\omega_p(q \to 0)$, as in the 2Deg, for accoustic plasmons, or in graphene, Eq. (10) ensures that the classical limit is reached $\propto \eta^2 \omega_p^2$. We therefore study the 2Deg in further detail, and compare the above approaches for the sheet plasmon.

3. Application to the 2Deg

The density n is related to the mean radius $r_S a_B = 1/\sqrt{n\pi}$, with an effective Bohr radius a_B. In typical semiconductor quantum wells $r_S \in [0.1, 10]$. Unless stated explicitly otherwise, we convert E_F into
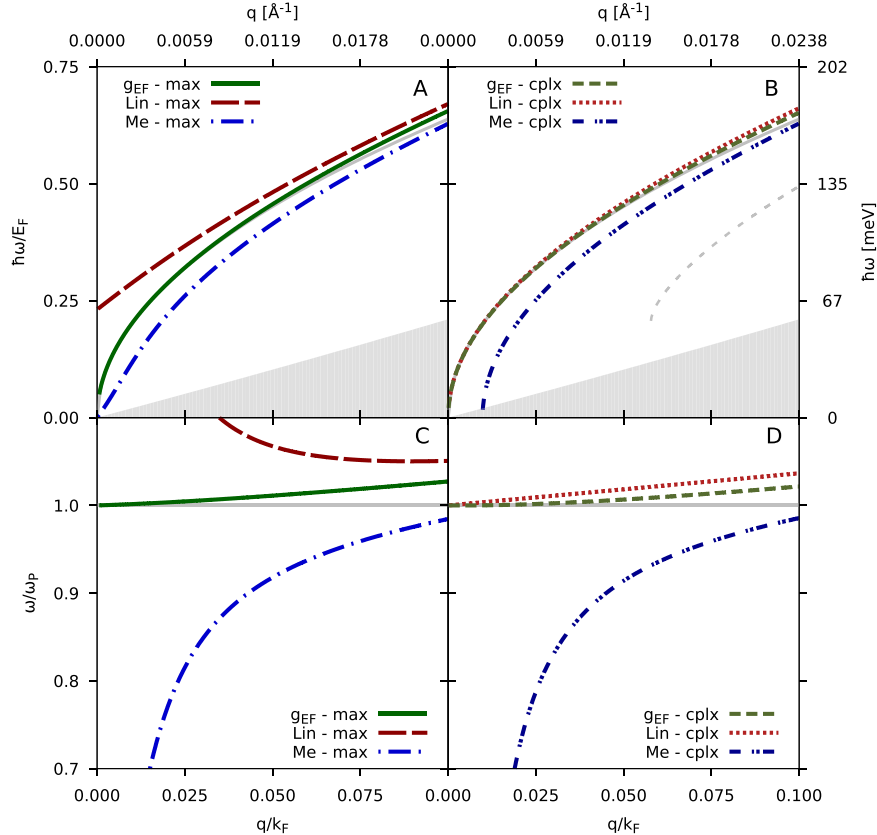

Fig. 1. (Color online) Plasmon dispersion ω_{pl} for $r_S = 1.44$ and $\hbar\eta = 0.4\,E_F$, obtained from Eqs.(1a) ('max') and (1b) ('cplx'). Mermin's results (dash-[double]dotted blue) from (6) are compared with those obtained from Eqs. (4) (dashed [A] and dotted [B] red) and (10) (full and dashed green). Light grey: Eq. (1c) with (6). Lower part: ω_{pl} divided by the classical $\omega_p \propto \sqrt{q}$. Upper part: ω_{pl} (both scales in E_F and eV hold for both parts A, B); shaded area: e/h band (Landau damping).
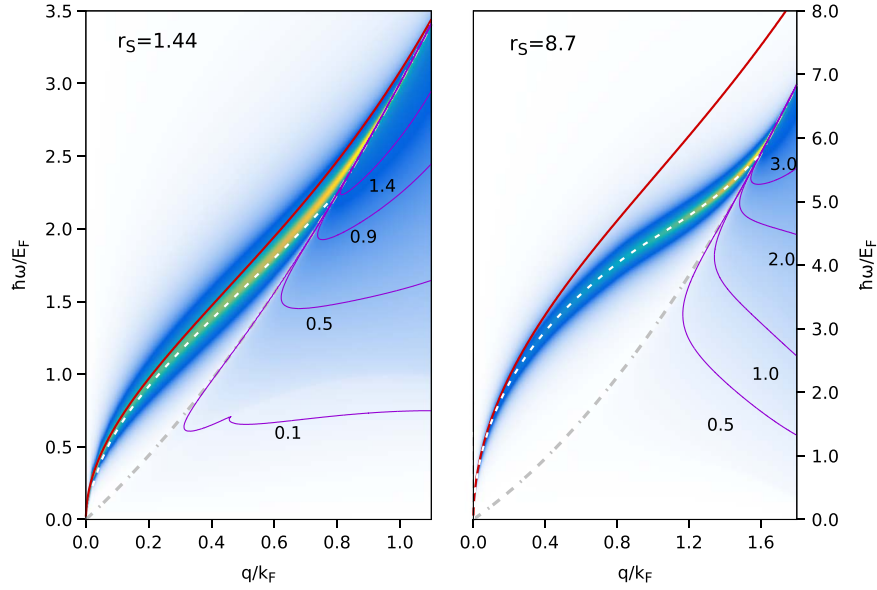
Fig. 3. (Color online) Contour plot of $-\mathrm{Im}\,\epsilon_g^{-1}(q,\omega)$ with (10) including screening (15) with $S(q)$ from [38]. Densities are chosen as realized in [14,16]. Red solid line: undamped bare RPA plasmon. White dashed line: Mermin's collective mode from (6) with V_{ph}. Grey dash–dotted line: upper e/h-band edge.
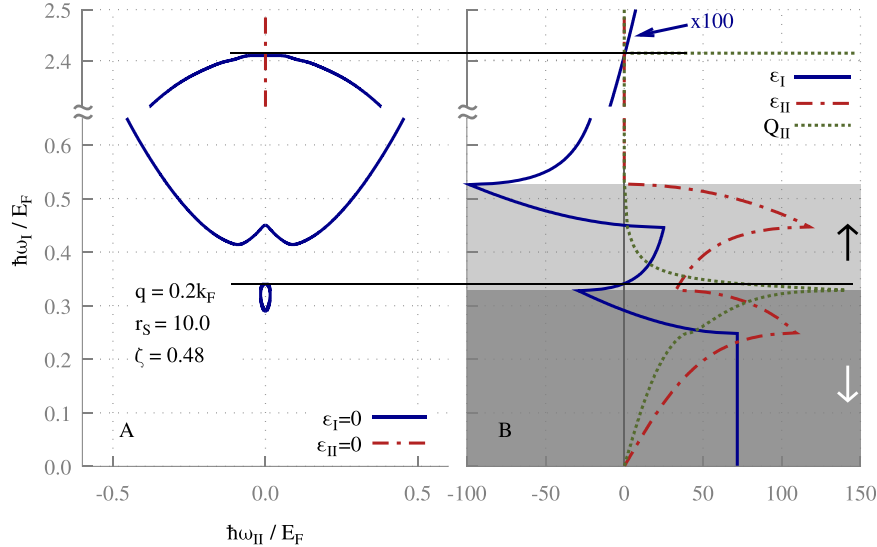

Fig. 4. (Color online) Spin plasmon determination in a 2Deg with $\lesssim 75\%$ spin-↑ electrons. (A) roots of ϵ_{I} (full blue line) and ϵ_{II} (dash-dotted red line) in the $\omega_{\mathrm{I}} + i\omega_{\mathrm{II}}$ plane. (B) Shaded regions with ↑ (↓) arrows indicate the e/h bands for spin-↑ (-↓) particles. Full blue and dash-dotted red line: Re and Im of $\epsilon(0.2k_{\mathrm{F}},\omega)$, respectively. Horizontal lines: density- and spin plasmon from $\epsilon_{\mathrm{I}} = 0$. Green dotted line: $-\mathrm{Im}\,v\,\chi_{ss}$.

eV for material parameters as given in Ref. [14] (a metallic $DySi_2$ monolayer on Si with $a_{\mathrm{B}}^* = 4.13$ Å, $n = 9 \cdot 10^{13}$ cm^{-2} corresponding to $E_{\mathrm{F}} = 269$ meV, Fermi wave vector $k_{\mathrm{F}} = 0.23$ Å^{-1}, and $r_s = 1.4$). An Ag monolayer also appears interesting [33].

In Fig. 1 the plasmon dispersions are shown for a fixed damping value of $\eta = 0.4\,E_{\mathrm{F}}/\hbar \approx 110$ meV/$\hbar$. We first compare the results from ϵ_{Lin} and ϵ_{Me}.

For $q \to 0$, both, $\omega_{\mathrm{pl}}^{(a)}(q)$ and $\omega_{\mathrm{pl}}^{(b)}(q)$ as defined in Eqs. (1a)–(1b), clearly deviate from the classical dispersion, $\omega_p = \sqrt{qne^2/2m\varepsilon_0}$. The Lindhard approach (4) (red lines in Fig. 1) yields an energy offset (long dashed line) via the maximum of the loss function, whereas ω_p and ω_{I} (dotted red line) from $\epsilon(q, \omega_{\mathrm{I}} + i\omega_{\mathrm{II}}) = 0$ almost coincide.

By contrast, the latter route gives a q-offset with Mermin's Eq. (6), (dash-double-dotted blue line), where roots only occur beyond some finite q (as first noted in [34]). From the absorption maximum a *linear* plasmon (dash-dotted blue line) follows, instead of $\propto\sqrt{q}$. The lower part of Fig. 1 makes this discrepancy evident. To our knowledge, no

such offsets have been yet observed.

The upper right part of Fig. 1 also shows the plasmon dispersion obtained from Re $\epsilon(q, \omega) = 0$ (grey dashed line). The result is depicted for ϵ_{Me}. Solutions exist only when both, ω as well as q, exceed some finite value. A big difference to the other curves is obvious. Significant deviations also arise with ϵ_{Lin}, ϵ_{g_1}, $\epsilon_{g_{\mathrm{D}}}$, small ones using $\epsilon_{g_{E_{\mathrm{F}}}}$.

The interpolation ansatz (10) (green curves) reproduces ω_p remarkably well via both routes (*cf.* Fig. 1 C, D). It thus appears to be the best choice.

Finally, (1d) yields a behavior (not displayed here) similar to (1a): ϵ_{Lin} giving an energy offset, ϵ_{Me} leading to the vanishing of $\omega_{\mathrm{pl}}^{(d)}(q \to 0)$ with a wrong order in q, and the results using g_{D} being close to those from ϵ_{Me}. Again, g_{D} obeys the classical limit, being a satisfying choice for the present purpose.

Half widths as large as ~ 500 meV ($\approx 5\%$ of the peak position) were reported in [12]. In graphene [19] even $\sim 50\%$ peak widths were found. Fig. 2 shows the predicted dispersions versus the damping parameter η

for a fixed wave vector. The difference between the results increases with the damping. Except for ϵ_{Lin} the dispersions decrease monotonically with η. A very close match holds for the ϵ_{Me} plasmons based on criterion (1a) or (1b).

For $\eta/\omega_{pl} \approx 10\%$ the differences are irrelevant, for $\eta/\omega_{pl} \approx 50\%$ the maximal distance amounts to $\sim 5\%$. In high resolution spectra of short-lived plasmons it therefore gets important, which expression is used for the plasmon.

The plain RPA is unreliable for higher q-values or dilute systems. Much effort has gone into improvements over the decades [1,35], reviewing them is beyond our scope. Commonly, a 'local field corrected' or effective potential $V(q) \equiv v(q)(1 - \mathcal{G}(q))$ is introduced in the dielectric function,

$$\epsilon_{GRPA} = 1 - \frac{v\chi^0}{1 + (1 - \mathcal{G}) \, v\chi^0}. \tag{14}$$

Choosing for V the particle–hole potential [36,37]

$$V_{ph}(q) = \frac{\hbar^2 q^2}{4mn}(S(q)^{-2} - S_0(q)^{-2}), \tag{15}$$

($S_0(q)$ is the non-interacting static structure factor [1]), has the advantage of changing the sum rules (13) and (11) only marginally. As $V_{ph}(q \to 0)$ simplifies to $v(q)$, the classical dispersion ω_p is recovered for undamped systems. A proper inclusion of correlation effects is ensured by using the state-of-the-art ground–state data for $S(q)$ (e.g. from [38,39]).

Correlations crucially lower the plasmon dispersion: in Fig. 3 the (yellow) maximum of the scattering loss function is significantly below the bare RPA result, Landau damping occurring at substantially lower q-vectors. The left part of Fig. 3 shows the same system as Fig. 1, in the more dilute case (right part) the effect is even more pronounced. There, $\hbar\eta = 0.4E_F = 0.05$ meV describes a relatively weaker damping (note the different $\omega-$ scales). The plasmon obtained from Eq. (1a) using ϵ_{Me} in the GRPA with V from (15) is found slightly lower (dashed line).

4. Spin plasmon

Another mode can exist in electron layers: the spin plasmon is the collective excitation of the longitudinal magnetization, proportional to the spin-density $s \equiv n_\uparrow - n_\downarrow$. Of negligible strength in Im ϵ^{-1}, it manifests itself in the spin-density response function χ_{ss}. It may be observed [40] in partially spin-polarized systems, as otherwise $\chi_{ss}^{RPA} = \chi^0$. Its dispersion lies inside the e/h band of the majority spins [37,40]. Hence Landau-damping establishes a substantial natural broadening mechanism, we add no artificial broadening, i.e. $\eta = 0$. Again, the mode can be defined either via (a generalized) criterion (1a) as a maximum in $-\text{Im}\,\chi_{ss}$, or via criterion (1b) as a zero of the denominator, in the RPA identical with $\epsilon(q, \omega)$. Such zeroes can be obtained graphically as intersections of the curves $\epsilon_I = 0$ and $\epsilon_{II} = 0$ in the complex ω-plane.

This is seen in Fig. 4. A for a 2Deg with a density of $r_S = 10$ and spin imbalance $s = 0.48\, n \equiv \zeta\, n$. For the conventional (charge-)density plasmon the intersection is clearly visible (due to $\eta = 0$ found at $\omega_{II} = 0$). The right part, Fig. 4.B, shows ϵ_I and ϵ_{II} vs. real ω (on the vertical axis), the top horizontal line marks the plasmon position. However, there is no (further) vanishing of ϵ_{II} within the majority e/h excitation band (light grey region). Though not a 'true' collective mode, in $-v(q)\,\text{Im}\,\chi_{ss}(q, \omega)$ (dotted green line) the spin plasmon is obvious as a sharp maximum *outside* the minority band; distinctly below the zero of ϵ_I. Again, Eqs. (1a,1c) yield noticeably different values.

5. Conclusion

We gave a brief overview on the formal properties of various response functions phenomenologically accounting for plasmon damping. Many common approaches do not exactly recover the classical limit. This can be ensured via Eqs. (10) and (8) in the 2Deg, where we quantitatively studied the influence of the damping on the dispersion. Special emphasis lay on the distinct results from different criteria; albeit small, this gets relevant with state-of-the-art measurements having reached the necessary resolution.

References

[1] G. Giuliani, G. Vignale, Quantum Theory of the Electron Liquid, Cambridge University Press, Cambridge, 2005.
[2] D. Pines, Elementary Excitations in Solids, Advanced Book Program, Perseus Books, Reading, Massachusetts, 1999.
[3] G.V. Naik, V.M. Shalaev, A. Boltasseva, Adv. Mater. 25 (2013) 3264–3294.
[4] J.B. Khurgin, Nat. Nanotechnol. 10 (2015) 2–6.
[5] N.D. Mermin, Phys. Rev. B 1 (1970) 2362–2363.
[6] H.T. Nguyen-Truong, J. Electron Spectrosc. Relat. Phenom. 193 (2014) 79–85.
[7] Y.V. Arkhipov, A.B. Ashikbayeva, A. Askaruly, A.E. Davletov, I.M. Tkachenko, Phys. Rev. E 90 (2014) 053102.
[8] E.M. Hankiewicz, G. Vignale, Y. Tserkovnyak, Phys. Rev. B 78 (2008) 020404.
[9] L. Zheng, S. Das Sarma, Phys. Rev. B 53 (1996) 9964–9967.
[10] M. Jablan, H. Buljan, M. Soljačić, Phys. Rev. B 80 (2009) 245435.
[11] M. Stöger-Pollach, Micron 39 (2008) 1092–1110.
[12] T. Nagao, T. Hildebrandt, M. Henzler, S. Hasegawa, Phys. Rev. Lett. 86 (2001) 5747–5750.
[13] T. Inaoka, T. Nagao, S. Hasegawa, T. Hildebrandt, M. Henzler, Phys. Rev. B 66 (2002) 245320.
[14] E.P. Rugeramigabo, T. Nagao, H. Pfnür, Phys. Rev. B 78 (2008) 155402.
[15] M. Eriksson, A. Pinczuk, B. Dennis, C. Hirjibehedin, S. Simon, L. Pfeiffer, K. West, Physica E 6 (2000) 165–168.
[16] C.F. Hirjibehedin, A. Pinczuk, B.S. Dennis, L.N. Pfeiffer, K.W. West, Phys. Rev. B 65 (2002) 161309.
[17] X. Hao, Z. Wang, M. Schmid, U. Diebold, C. Franchini, Phys. Rev. B 91 (2015) 085204.
[18] Z. Fei, G.O. Andreev, W. Bao, L.M. Zhang, A.S. McLeod, C. Wang, M.K. Stewart, Z. Zhao, G. Dominguez, M. Thiemens, M.M. Fogler, M.J. Tauber, A.H. Castro-Neto, C.N. Lau, F. Keilmann, D.N. Basov, Nano Lett. 11 (2011) 4701–4705.
[19] T. Langer, J. Baringhaus, H. Pfnür, H.W. Schumacher, C. Tegenkamp, New J. Phys. 12 (2010) 033017.
[20] S.D. Sarma, Q. Li, Solid State Commun. 152 (2012) 1795–1799.
[21] K. Kechedzhi, S. Das Sarma, Phys. Rev. B 88 (2013) 085403.
[22] S.Y. Shin, N.D. Kim, J.G. Kim, K.S. Kim, D.Y. Noh, K.S. Kim, J.W. Chung, Appl. Phys. Lett. 99 (2011).
[23] A.N. Grigorenko, M. Polini, K.S. Novoselov, Nat. Photon. 6 (2012) 749–758.
[24] F.J.G. de Abajo, ACS Photon. 1 (2014) 135–152.
[25] G. Röpke, Phys. Rev. E 57 (1998) 4673–4683.
[26] A. Selchow, G. Röpke, A. Wierling, H. Reinholz, T. Pschiwul, G. Zwicknagel, Phys. Rev. E 64 (2001) 056410.
[27] H. Reinholz, R. Redmer, G. Röpke, A. Wierling, Phys. Rev. E 62 (2000) 5648–5666.
[28] G.S. Atwal, N.W. Ashcroft, Phys. Rev. B 65 (2002) 115109.
[29] H.M. Böhm, R. Holler, E. Krotscheck, M. Panholzer, Phys. Rev. B 82 (2010) 224505.
[30] H. Mendlowitz, J. Opt. Soc. Am. 50 (1960) 739–740.
[31] L.J.P. Ament, M. van Veenendaal, T.P. Devereaux, J.P. Hill, J. van den Brink, Rev. Mod. Phys. 83 (2011) 705–767.
[32] P. Coleman, Introduction to Many-Body Physics, Cambridge University Press, Cambridge, 2015.
[33] V.M. Silkin, T. Nagao, V. Despoja, J.P. Echeverry, S.V. Eremeev, E.V. Chulkov, P.M. Echenique, Phys. Rev. B 84 (2011) 165416.
[34] G.F. Giuliani, J.J. Quinn, Phys. Rev. B 29 (1984) 2321–2323.
[35] N. Bhukal, Priya, R. Moudgil, Physica E 69 (2015) 13–18.
[36] E. Krotscheck, in: A. Fabrocini, S. Fantoni, E. Krotscheck (Eds.), Introduction to Modern Methods of Many-Body Theory and their Applications, Advances in Quantum Many-Body Theory, vol. 7, World Scientific, Singapore, 2002, pp. 267–330.
[37] D. Kreil, R. Hobbiger, J.T. Drachta, H.M. Böhm, Phys. Rev. B 92 (2015) 205426.
[38] P. Gori-Giorgi, S. Moroni, G.B. Bachelet, Phys. Rev. B 70 (2004) 115102.
[39] R. Asgari, B. Davoudi, M. Tosi, Solid State Commun. 131 (2004) 301–305.
[40] A. Agarwal, M. Polini, G. Vignale, M.E. Flatté, Phys. Rev. B 90 (2014) 155409.